Understanding the Variations of the Length and the Seasonal Rainfall Anomalies of the Indian Summer Monsoon

VASUBANDHU MISRA

Center for Ocean–Atmospheric Prediction Studies, Department of Earth, Ocean and Atmospheric Science, and Florida Climate Institute, Florida State University, Tallahassee, Florida

AMIT BHARDWAJ AND RYNE NOSKA

Center for Ocean–Atmospheric Prediction Studies, and Florida Climate Institute, Florida State University, Tallahassee, Florida

(Manuscript received 12 July 2016, in final form 22 November 2016)

ABSTRACT

The canonical relationship between the length and the total seasonal rainfall anomalies of the Indian summer monsoon (ISM) is the association of the longer (shorter) season with wetter (drier) seasonal rainfall anomalies. This study shows that such canonical behavior is clearly associated with relatively strong ENSO SST anomalies in the eastern equatorial Pacific Ocean that appear in the boreal summer and fall seasons. The noncanonical relationship is caused by a longer (shorter) season associated with drier (wetter) ISM seasonal rainfall anomalies. A majority of these noncanonical seasons, with anomalously short season length but anomalously high seasonal mean rain, tend to occur under relatively weak La Niña forcing during the boreal summer season. Although the onset of such seasons occurs through canonical ENSO forcing of a large-scale meridional temperature gradient, the demise is dictated by the depletion of moist static energy from the underlying cooling of the upper ocean in the northern Indian Ocean. This is due to stronger meridional Ekman ocean heat transport forced by the stronger low-level atmospheric southwesterlies than those in the corresponding canonical wet ISM season.

1. Introduction

The robust seasonal cycle of the Indian summer monsoon (ISM) is characterized by the dramatic onset of rains and its systematic withdrawal (Koteswaram 1958; Ramage 1971; Ananthakrishnan and Soman 1988). This seasonality of the ISM has been observed for several centuries from paleorecords (Yadava et al. 2004). Furthermore, some of the recent studies have clearly shown that variations of the length of the ISM season are as important as the variations in the seasonal mean rain rate of the ISM (Xavier et al. 2007; Sperber and Annamalai 2014; Noska and Misra 2016). In fact, Xavier et al. (2007) suggest that the teleconnection between variations of ENSO and length of the ISM season (as diagnosed by the reversal of the meridional gradient of the mid- to upper-tropospheric temperature in the southern Eurasian region) is more stable over time than ENSO and mean seasonal rain-rate anomalies of the ISM over the fixed calendar months of June–September.

Noska and Misra (2016) show that variations of the onset and demise of the ISM rainfall are related to large-scale changes in the regional atmospheric and oceanic circulation and the regional ocean–atmosphere thermal gradients. For example, Noska and Misra (2016) show that their definition of onset/demise of the ISM based on all-India-averaged rainfall (AIR) is related to the upper-level temperature gradient that reverses from a negative to a positive value at the time of onset of the ISM (Yanai et al. 1992). More recently, Parker et al. (2016) show that the advance of the onset of the ISM also coincides with midlevel dry air intrusion from the northwest. Similarly, Noska and Misra (2016) show that onset/demise date variations of ISM rainfall are also related to the variability of the cross-equatorial upper-ocean heat transport in the tropical Indian Ocean. In this study we seek to understand the relationship between the variations of the length of the ISM with its seasonal rainfall variations on the interannual time scale. We define a canonical

Corresponding author e-mail: Vasubandhu Misra, vmisra@fsu.edu

DOI: 10.1175/JCLI-D-16-0501.1

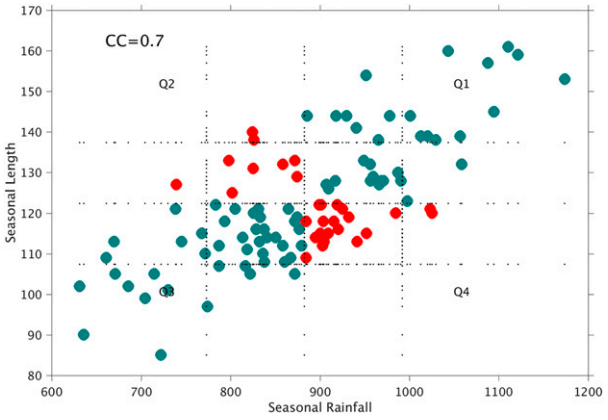

FIG. 1. The scatter between seasonal length (Julian days) and seasonal accumulation of rainfall (mm) of the ISM for 104 years (1902–2005). The green (red) dots refer to the canonical (non-canonical) ISM seasons in the relation between season length and seasonal accumulated rainfall (see text). The mean and the one std dev about the mean for the variable represented along the ordinate and abscissa are indicated by the dotted lines. The four quadrants of these scatterplots bounded by the mean of the abscissa and ordinate variables are labeled $Q1$, $Q2$, $Q3$, and $Q4$. The correlation (CC) between the variables of the scatterplot is also indicated.

relationship between the seasonal length and the total seasonal rainfall anomalies of the ISM when longer (shorter) than mean season length is associated with wetter (drier) than mean seasonal rainfall of the ISM. Similarly, we call the relationship noncanonical when longer (shorter) than mean season length is associated with drier (wetter) than average ISM seasonal rainfall. We shall characterize the features of such canonical and noncanonical ISM seasons in this study. In the following section, we briefly discuss the datasets used followed by the discussion of results in section 3 with concluding remarks in section 4.

2. Datasets and methods

We have used four datasets in this study: daily rain gauge–based analysis over India produced by the Indian Meteorological Department (IMD; Pai et al. 2014, 2015); the daily upper-air variables from the twentieth century reanalysis from the European Centre for Medium-Range Weather Forecasts (ERA-20C; Poli et al. 2013); the monthly oceanic heat content from the centennial ocean analysis of Simple Ocean Data Assimilation, version 2.2.4 (SODA; Carton and Giese 2008); and the Extended Reconstructed SST, version 3b (ERSST.v3b; Smith et al. 2008). The IMD rainfall dataset is available daily at 0.25° × 0.25° grid spacing from 1902 to 2005. Similarly, upper-air variables from ERA-20C at T159 spectral resolution (~1.0° × 1.0° grid spacing) and SST from ERSST.v3b are available daily at 2.0° × 2.0° grid spacing from 1850 to present. The depth of the 20°C isotherm used as a proxy for ocean heat content (Kessler 1990; Meinen and McPhaden 2000) is obtained from monthly subsurface ocean temperatures from SODA, available at 0.5° grid spacing on 40 z levels for the period 1901–2008. All our analysis is based on the overlapping period of the IMD rain gauge dataset.

Noska and Misra (2016) have uniquely defined the onset and demise of the ISM based on the AIR. They argue that such an areal average over all of India is necessary to avoid diagnosis of false onset and demise of the ISM from synoptic- or mesoscale events that are unrelated to the seasonal evolution of the ISM. They define the onset of the ISM as the first day of the year after the daily accumulated anomaly of AIR (computed against the climatological annual mean AIR) reaches the absolute minimum. Similarly, they define the demise of the ISM as the first day of the year after the daily accumulated anomaly of AIR (computed against the climatological annual mean AIR) reaches the absolute maximum. We use similar definitions of the onset and demise of the ISM for this study.

For examining the statistical significance of our results we resort to using the nonparametric bootstrapping technique for statistical significance (Wilks 2011). In this method the time series is randomly resampled 1000 times (with replacement) to generate a distribution of the metric to be tested (e.g., composite anomalies). Then, for example, the anomaly computed from the sample time series is considered significant at the 90% confidence interval if the anomaly lies within the 5th or beyond the 95th percentile of the distribution of the anomalies. This method is widely used for significance tests (e.g., Mo 2010; Misra et al. 2014; Yuan et al. 2015).

3. Results

a. *Variations of seasonal length and total seasonal rainfall*

The canonical and noncanonical behavior of the ISM seasonal rainfall and its seasonal length are best illustrated in Fig. 1. It shows the scatter between the ISM seasonal length and the total seasonal rainfall. It should be noted that the total seasonal rainfall in Fig. 1 is computed by accumulating daily rain (mm day^{-1}) between the onset and the demise dates of the ISM for each year. The canonical seasons in Fig. 1 are identified by the green dots that conform with similar signs in the anomalies of the seasonal length and rainfall. Similarly, the red dots in Fig. 1 indicate the noncanonical seasons, where the sign of the anomalies of seasonal rainfall and length are conflicting. The ISM is noncanonical in 29 of

TABLE 1. Mean and std dev of the various features of the ISM seasons in the four quadrants of Fig. 1a.

Quadrant season (from Fig. 1a)	Onset date		Demise date		Season length		Seasonal rain	
	Mean (days)	Std dev (days)	Mean (days)	Std dev (days)	Mean (days)	Std dev (days)	Mean (mm)	Std dev (days)
*Q*1	150.5	10.8	289.2	13.4	138.8	20.1	994.3	133.1
*Q*2	153.3	6.8	285.3	10.9	132	11.3	824.4	74.8
*Q*3	159.2	7.3	269.8	12.3	110.6	14.5	791.4	116.6
*Q*4	160.1	6.3	277.2	6.3	117.2	6.6	926.2	60.7
All	156.2	8.2	278.6	11.5	122.4	15	882.6	109.5

the 104 years (nearly 28% of the years). However, in the majority of these noncanonical years the anomalies of seasonal length and rainfall are below one standard deviation unlike in the canonical years when anomalies for several seasons are significantly larger than one standard deviation. In Fig. 1 we have marked the four quadrants *Q*1, *Q*2, *Q*3, and *Q*4, representing ISM seasons with anomalously long and more, long and less, short and less, and short and more seasonal length and rainfall, respectively. It may be noted that a majority (20) of the noncanonical seasons reside in *Q*4 (i.e., seasons with anomalously short length but wet seasonal rainfall anomalies of the ISM). On the other hand, a majority of the canonical seasons (43) reside in *Q*3 (i.e., seasons with anomalously short length and drier seasonal rainfall of the ISM). In contrast, only 9 (32) noncanonical (canonical) seasons reside in *Q*2 (*Q*1) [i.e., seasons with anomalously long length but dry (wet) seasonal rainfall anomalies of the ISM].

Table 1 clearly affirms that the deviations of the seasonal length and rainfall for the canonical seasons in *Q*1 and *Q*3 relative to the climatology are much larger than the noncanonical seasons residing in *Q*2 and *Q*4. However, the variability of onset and demise dates, seasonal length, and seasonal rainfall within the two types of canonical (noncanonical) seasons of *Q*1 and *Q*3 (*Q*2 and *Q*4) are comparable to each other.

As pointed out in Noska and Misra (2016), the variations of the onset date and demise date of the ISM has a bearing on the seasonal rainfall anomaly of the ISM. This is also shown in terms of the correlations of the anomalies of dates of onset (Fig. 2a) and demise (Fig. 2b) with the succeeding and preceding ISM rainfall anomalies, respectively. It is apparent from Fig. 2a that an early (late) onset date of the ISM is associated with higher (lower) seasonal rainfall anomaly of the ISM. It may be noted that anomalous early (late) onset dates are ascribed with negative (positive) anomaly. Likewise, an early (late) demise date of the ISM is associated with lower (higher) seasonal rainfall anomaly of the ISM (Fig. 2b). Here, positive (negative) anomalies of demise date are attributed to later (early) demise of the ISM. The correlations are however slightly stronger with the onset date variations (Fig. 2a) than with the demise date variations (Fig. 2b), which all the more raises the significance of monitoring the onset of the ISM that can also serve as a harbinger of the forthcoming ISM season. These relationships are maintained in the canonical years (Figs. 2c,d). In contrast, in the noncanonical years this relationship completely breaks down (Figs. 2e,f) with correlations opposite in sign over central India (core ISM region) to that displayed by all and canonical years (Fig. 2d). Therefore, understanding noncanonical ISM seasons is critical to avoid incorrect interpretations of onset, demise, and seasonal length of the ISM.

b. Relation with ENSO

Several studies have established a robust relationship between AIR and Niño-3.4 SST anomalies (Sikka 1980; Angell 1981; Shukla and Paolino 1983), with maximum correlation occurring with the former leading the latter by a season (Krishnamurthy and Kinter 2003). A similar relationship between the total seasonal rainfall anomaly of the ISM and Niño-3.4 monthly SST anomaly is shown in Fig. 3a. In comparison, the seasonal length anomalies of ISM have weaker (but significant) correlations with the Niño-3.4 SST anomalies, are maximum (in magnitude) contemporaneously [i.e., in the June–August (JJA) season], and decrease slightly in subsequent months (Fig. 3a).

Qualitatively similar correlations are observed for the canonical ISM seasons (Fig. 3b) with an important difference that the magnitude of the correlations is slightly higher than those in Fig. 3a. However, in the noncanonical ISM seasons (Fig. 3c), there is a near-total collapse of the relationship of the seasonal length with Niño-3.4 SST anomalies. But the total seasonal AIR anomaly continues to sustain a robust negative correlation in August–November, consistent with canonical seasons (Fig. 3c). The majority of the ISM seasons, either canonical or noncanonical, occur when ENSO is in transition from one phase to the other from the preceding winter to the following fall season (Fig. 4). It may be noted, however, that a majority (17) of the

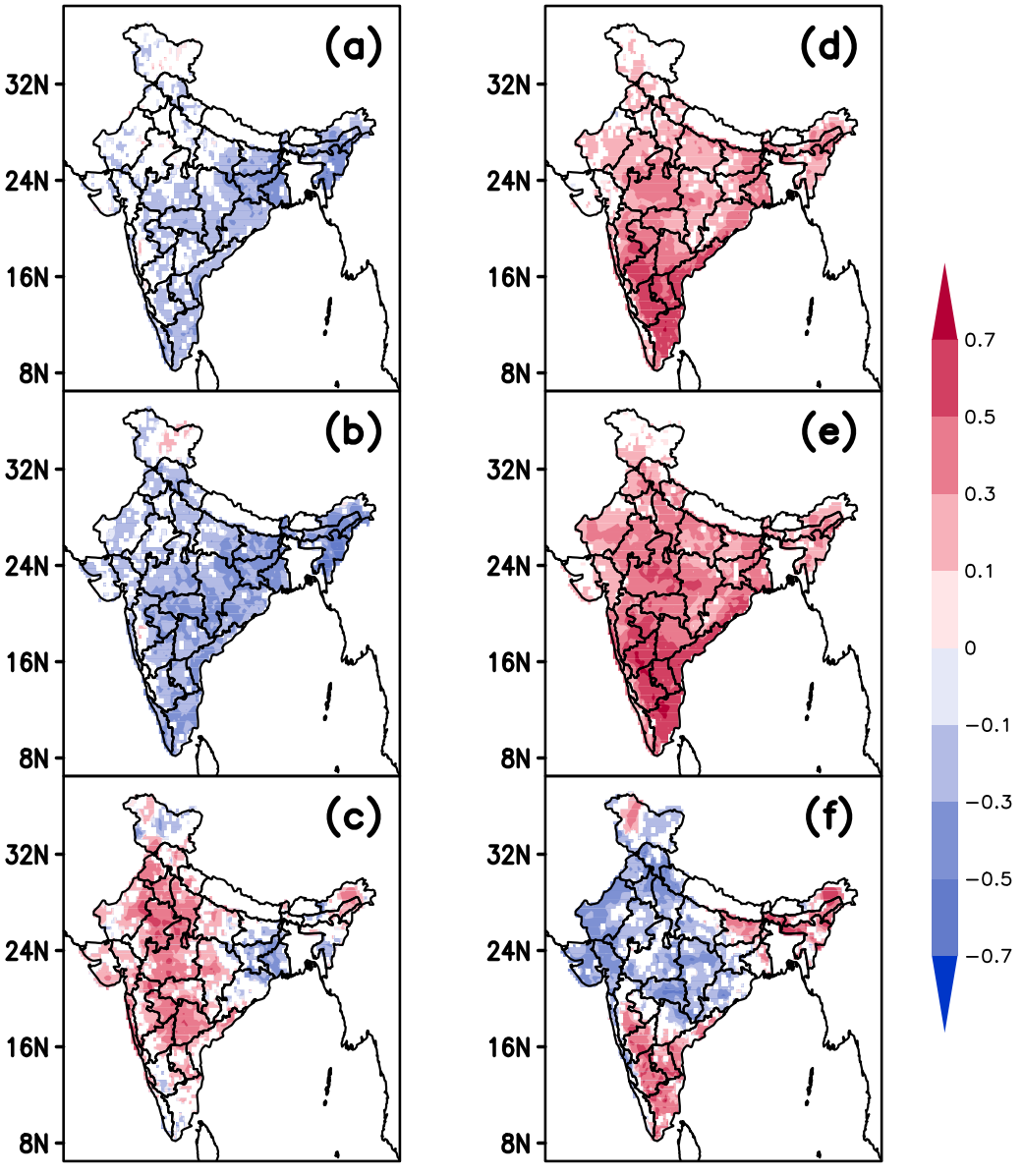

FIG. 2. The correlation of onset date of ISM with the seasonal rainfall anomalies of ISM for (a) all, (b) canonical, and (c) noncanonical years. Similarly, the correlation of demise date of ISM with the seasonal rainfall anomalies of ISM for (d) all, (e) canonical, and (f) noncanonical years. Significant values at the 10% significance level are shaded.

noncanonical (*Q*4) seasons occur when colder SST anomalies are observed in the Niño-3.4 region during the JJA season and are preceded by warm anomalies in the Niño-3.4 region in the DJF season (Fig. 4). It is interesting to note that the canonical and noncanonical seasons of ISM for weaker ENSOs are nearly non-discriminating (Fig. 4). In other words, weak ENSOs can be associated with either canonical or noncanonical ISMs. However, a clear majority of strong ENSO events are associated with canonical ISMs, with a minority of exceptions associated with noncanonical ISMs (Fig. 4).

c. *Large-scale meridional temperature gradient*

Several studies have shown that the seasonality of the ISM is associated with the reversal of the large-scale temperature gradient between the Tibetan Plateau and the neighboring oceans (Yanai et al. 1992; Webster et al. 1998; Noska and Misra 2016). Many studies have also related this temperature gradient reversal to the

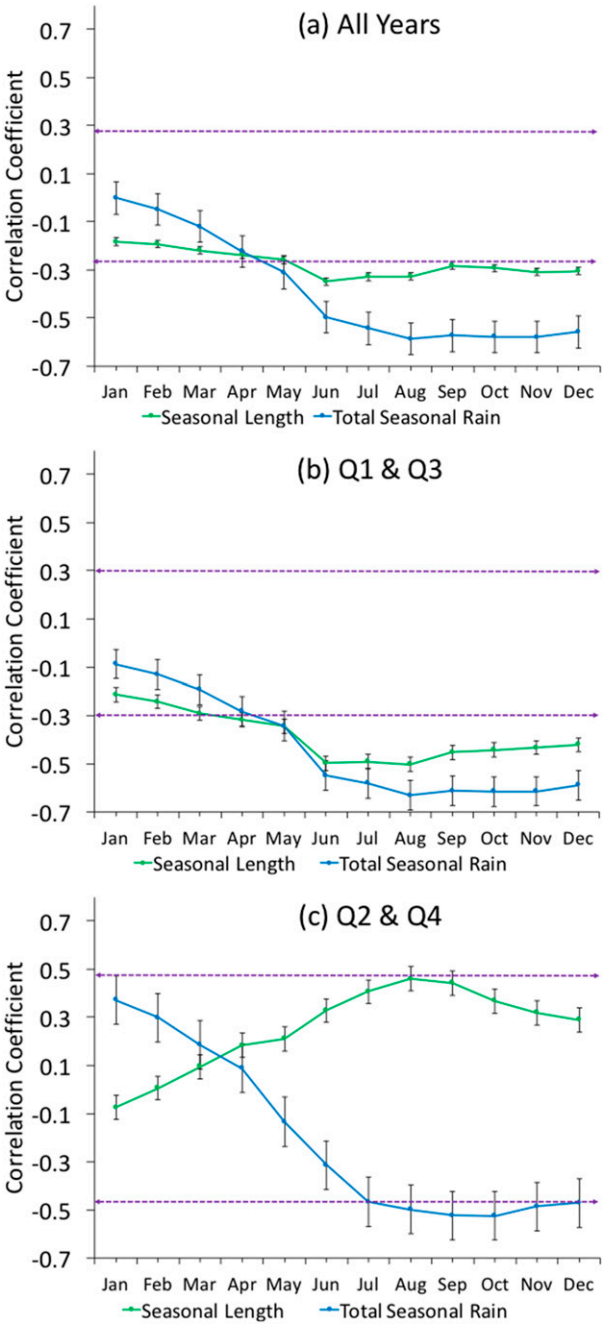

FIG. 3. The correlation of the monthly Niño-3.4 SST anomalies from ERSST.v3b and seasonal length and total seasonal rain of the ISM for (a) all seasons, (b) canonical seasons ($Q1$ and $Q3$ in Fig. 1), and (c) noncanonical seasons ($Q2$ and $Q4$ in Fig. 1). The purple dashed lines indicate the 10% significance level according to a Student's t test.

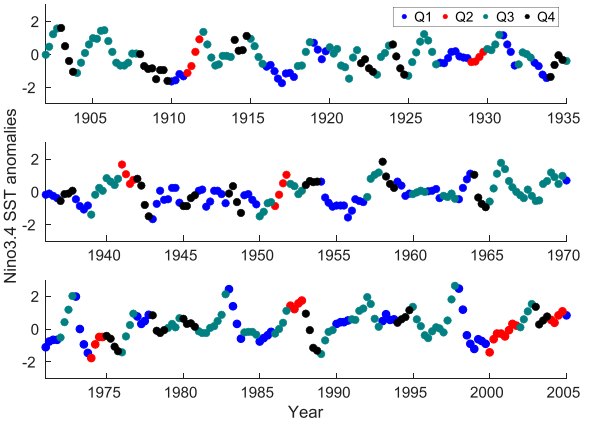

FIG. 4. Time series of the seasonal mean Niño-3.4 SST anomalies from ERSST.v3b. The time series is color marked for the preceding DJF and MAM, contemporaneous JJA, and following SON seasonal mean Niño-3.4 SST anomalies by the ISM season belonging to one of the four quadrants in Fig. 1.

initiation of moist symmetric instability of the ISM (Tomas and Webster 1997; Krishnakumar and Lau 1998; Goswami and Xavier 2005). It is posited in these studies that the significant premonsoon heating over the continental region establishes a large-scale cyclonic vorticity in the lower troposphere that results in the zero line of the absolute vorticity to shift north of the equatorial Indian Ocean, making the condition thereby conducive for moist symmetric instability that enables the onset of the ISM rains. Figures 5a–c show the correlations of the onset date of the ISM season with the temperature gradient (300-hPa temperature difference between 25° and 5°N) for all, canonical, and noncanonical ISM seasons. In all (Fig. 5a) and canonical (Fig. 5b) ISM seasons, an anomalous stronger (weaker) 300-hPa temperature gradient between 40°–70° and 70°–120°E appears, preceding the onset date of the ISM by ~20 and ~60–20 days, respectively. The onset date of the ISM is also succeeded (by ~40 days) by similar temperature gradient anomalies over the longitudinal range of 40°–70°E. A similar relationship is observed even in the noncanonical seasons (Fig. 5c) but with an important difference that significant correlations over 40°–70°E lag/lead by half as many days (~10 days preceding and ~20 days succeeding the onset date of the ISM). Furthermore, correlations in the longitude range of the Tibetan Plateau (70°–120°E) are insignificant for the noncanonical seasons (Fig. 5c). These relationships in Figs. 5a–c are essentially maintained by the remote ENSO forcing as similar correlations are observed when the temperature gradient is correlated with the preceding DJF Niño-3.4 SST anomalies (Figs. 5d–f) with the exception that ENSO modulation of the temperature gradient in the 70°–120°E longitudinal range is apparent in Fig. 5f.

Similarly, in all (Fig. 6a) and canonical (Fig. 6b) ISM seasons, the late (early) demise of the ISM season is

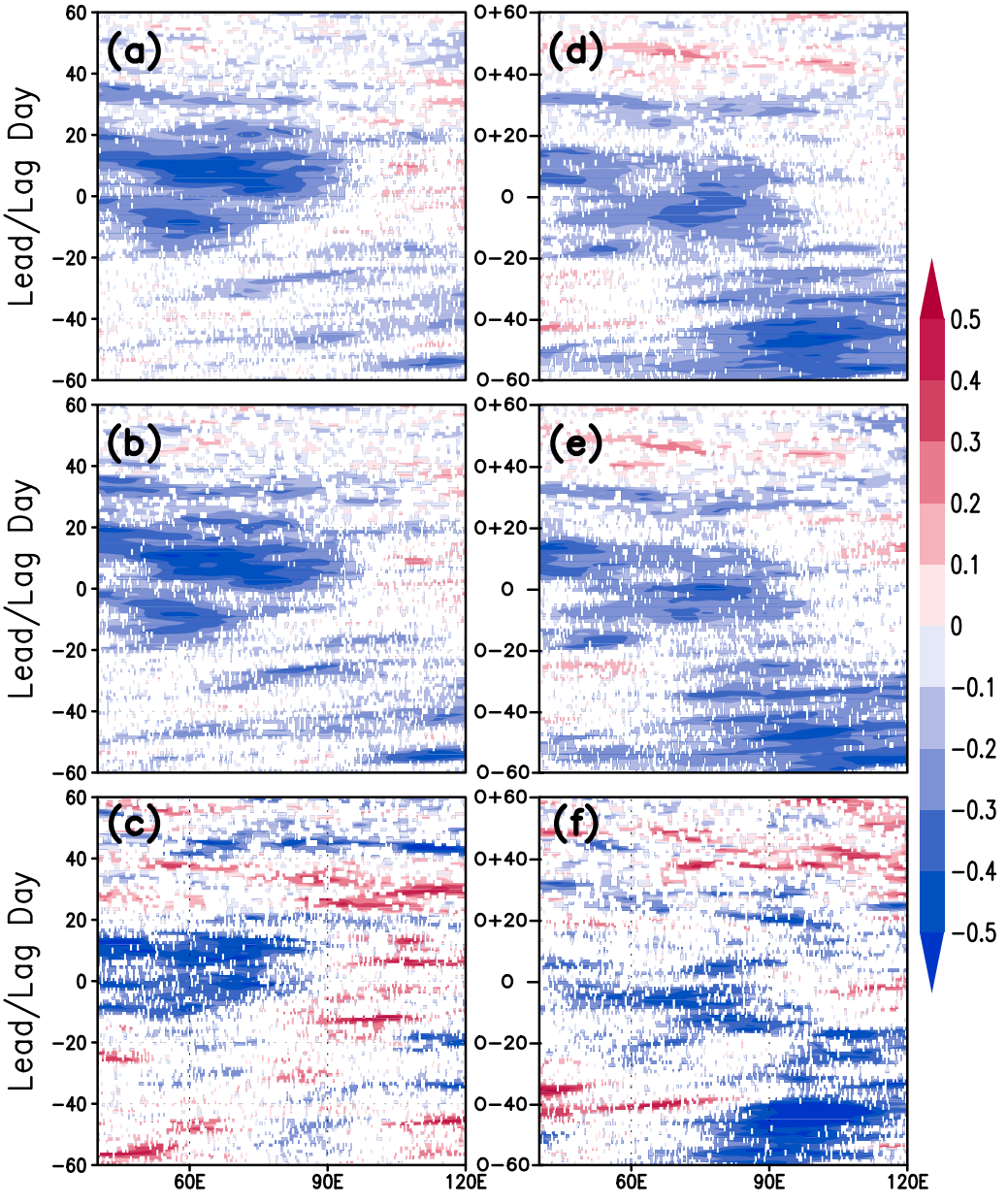

FIG. 5. Correlations of the onset date of the ISM season with meridional temperature gradient computed as the difference between 5° and 25°N for (a) all, (b) canonical, and (c) noncanonical ISM seasons. Negative (positive) values along the *y* axis in (a)–(c) indicate onset date lagging (leading) the meridional temperature gradient (days). Similarly, correlations of the preceding mean DJF Niño-3.4 SST anomalies with meridional temperature gradient computed as the difference between 5° and 25°N for (d) all, (e) canonical, and (f) noncanonical ISM seasons. The range from $O - 60$ to $O + 60$ along the *y* axis in (d)–(f) is the range of 60 days before and 60 days after the onset (day O) of the ISM season, respectively. Only significant values at the 10% significance level are shaded.

associated with a near-simultaneous stronger (weaker) temperature gradient at 300 hPa over a longitude domain of 40°–90°E. This relationship is comparatively weak in the noncanonical ISM seasons (Fig. 6c). Again, these relationships in all (Fig. 6d) and canonical (Fig. 6e) seasons are maintained from remote ENSO forcing except in the noncanonical ISM seasons, when the correlations are comparatively weaker (Fig. 6f).

d. Mechanism for noncanonical ISM season

We will focus to understand the *Q*4 seasons. As noted earlier, *Q*4 seasons carry a majority of the noncanonical

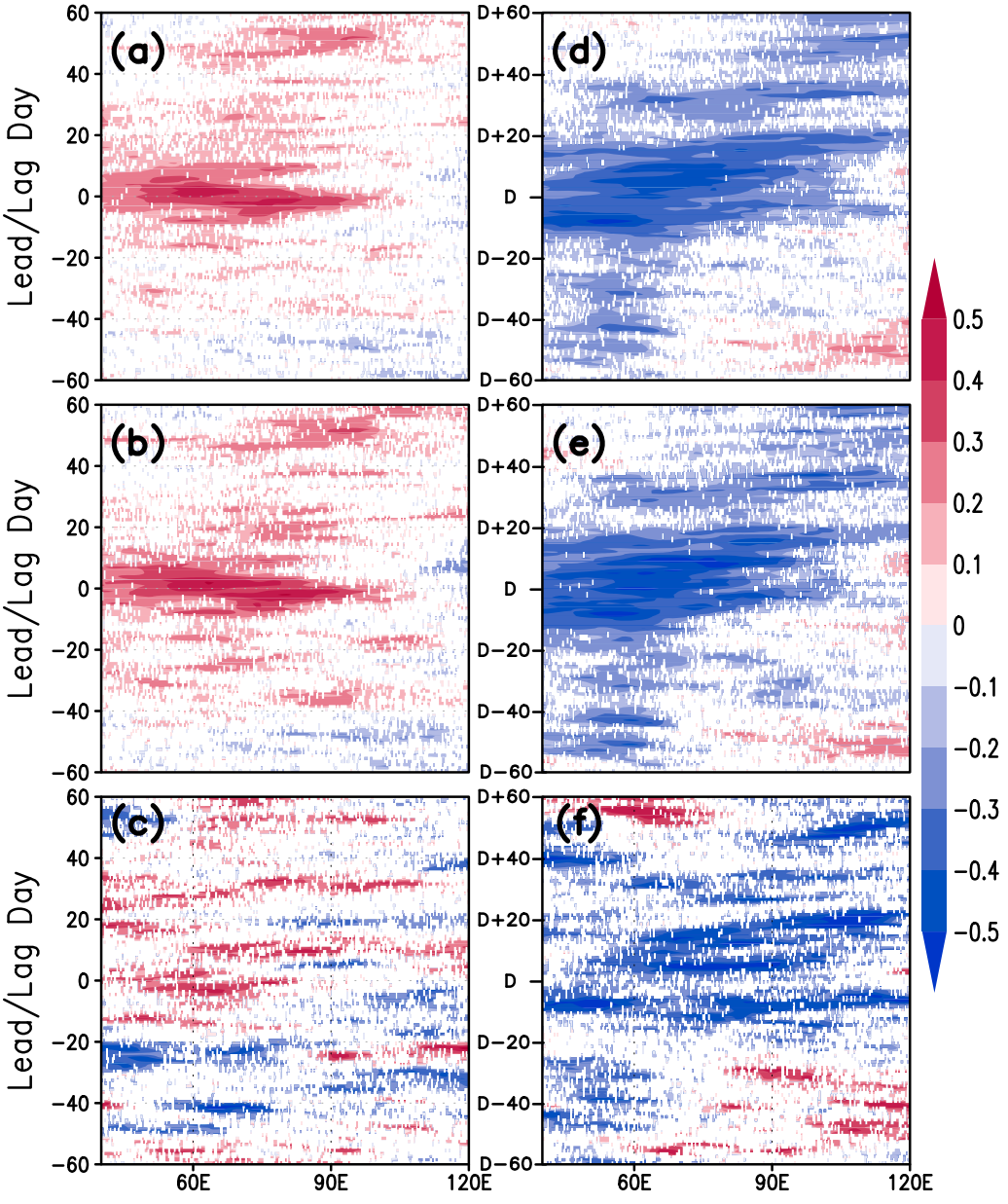

FIG. 6. Correlations of the demise date of the ISM season with meridional temperature gradient computed as the difference between 5° and 25°N for (a) all, (b) canonical, and (c) noncanonical ISM seasons. Negative (positive) values along the y axis in (a)–(c) indicate demise date lagging (leading) the meridional temperature gradient (days). Similarly, correlations of the mean JJA Niño-3.4 SST anomalies with meridional temperature gradient computed as the difference between 5° and 25°N for (d) all, (e) canonical, and (f) noncanonical ISM seasons. The range from $D - 60$ to $D + 60$ along the y axis in (d)–(f) is the range of 60 days before and 60 days after the demise (day D) of the ISM season, respectively. Only significant values at the 10% significance level are shaded.

ISM seasons, which are largely characterized by later onset and earlier demise of the ISM season. We will compare the canonical ISM seasons of $Q1$ and the noncanonical seasons of $Q4$ to develop an understanding of noncanonical behavior of the ISM as both seasons feature anomalously more seasonal rain but the former with longer and the latter with shorter length of the ISM season. The later onset of the $Q4$ seasons is largely a result of the preceding warm ENSO forcing (Fig. 4). However, the anomalously early demise of the $Q4$ season despite favorable ENSO forcing for later demise is a result of the relative depletion of the

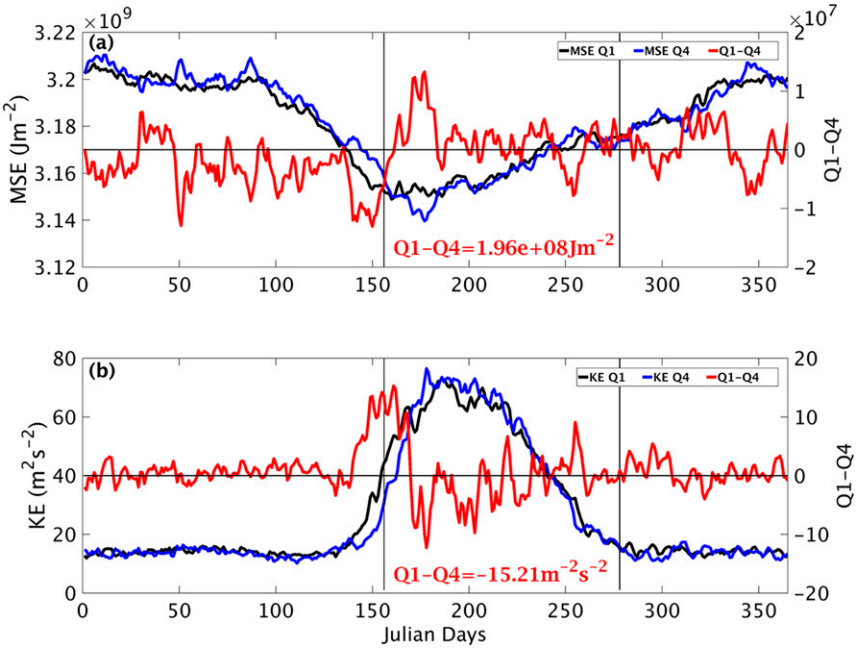

FIG. 7. Composite area-averaged (8°–30°N, 60°–95°E) time series of (a) daily moist static energy and (b) kinetic energy at 850 hPa for the $Q1$ (black line) and $Q4$ (blue line) seasons and their corresponding difference ($Q1 - Q4$; in red). The climatological seasonal mean difference of the moist static energy and the kinetic energy computed between the onset and demise dates of the ISM are also indicated in (a) and (b), respectively. The vertical gray lines in the two panels represent the climatological onset and demise of the ISM season. The net climatological seasonal difference between the two types of seasons ($Q1 - Q4$) is also indicated in each panel.

moist static energy compared to $Q1$ seasons (Fig. 7a). In Fig. 7a we show the daily climatological average of the vertically integrated moist static energy averaged over India for $Q1$ and $Q4$ seasons. We observe in Fig. 7a that $Q4$ seasons have an overall lower seasonal moist static energy in the ISM season. The moist static energy is initially large in $Q1$ compared to $Q4$, consistent with the early onset of the ISM in the former (canonical) seasons. Subsequently the differences between the two types of seasons oscillate about the zero line with a brief decrease in $Q1$ compared to $Q4$ before the demise of the ISM. This is a result of stronger low-level southwesterlies that develop soon after onset of the ISM season, which manifests in higher 850-hPa kinetic energy in the early part of the $Q4$ seasons (which have later onset) relative to the $Q1$ season (Fig. 7b). We observe that in the initial part of the season the kinetic energy is higher in the $Q1$ season (which has earlier onset). But subsequently the kinetic energy in $Q1$ is lower relative to the $Q4$ season giving a net increase in seasonal kinetic energy in the $Q4$ season relative to the $Q1$ season. As a result, there is more meridional Ekman ocean heat transport (not shown but implied) by the stronger forcing of the atmospheric southwesterlies in the $Q4$ season (Webster 2000; Chirokova and Webster 2006), resulting in less heat content in the northern Indian Ocean during the ISM season compared to $Q1$ seasons (Fig. 8). Consequently, in the noncanonical $Q4$ seasons, the ISM has to terminate early with the depletion of moist static energy from the cooling of the northern Indian Ocean relative to the $Q1$ season despite favorable ENSO forcing on the meridional temperature gradient for a delayed demise (Fig. 6f).

4. Conclusions

The variations of the length and the onset of the ISM and its implication on the seasonal rainfall variations are important features of the ISM. We relate canonical ISM seasons when a longer than mean (shorter than mean) season is associated with wetter (drier) than mean seasonal rainfall. Similarly, the noncanonical ISM seasons occur when a longer (shorter) than mean season is associated with drier (wetter) than mean ISM seasonal rainfall. Identifying and understanding such noncanonical seasons from the canonical seasons of the ISM is important. For example, the variation of the onset date of the ISM about its climatology, which can be potentially used to understand the variations of the subsequent ISM seasonal rain in the canonical seasons,

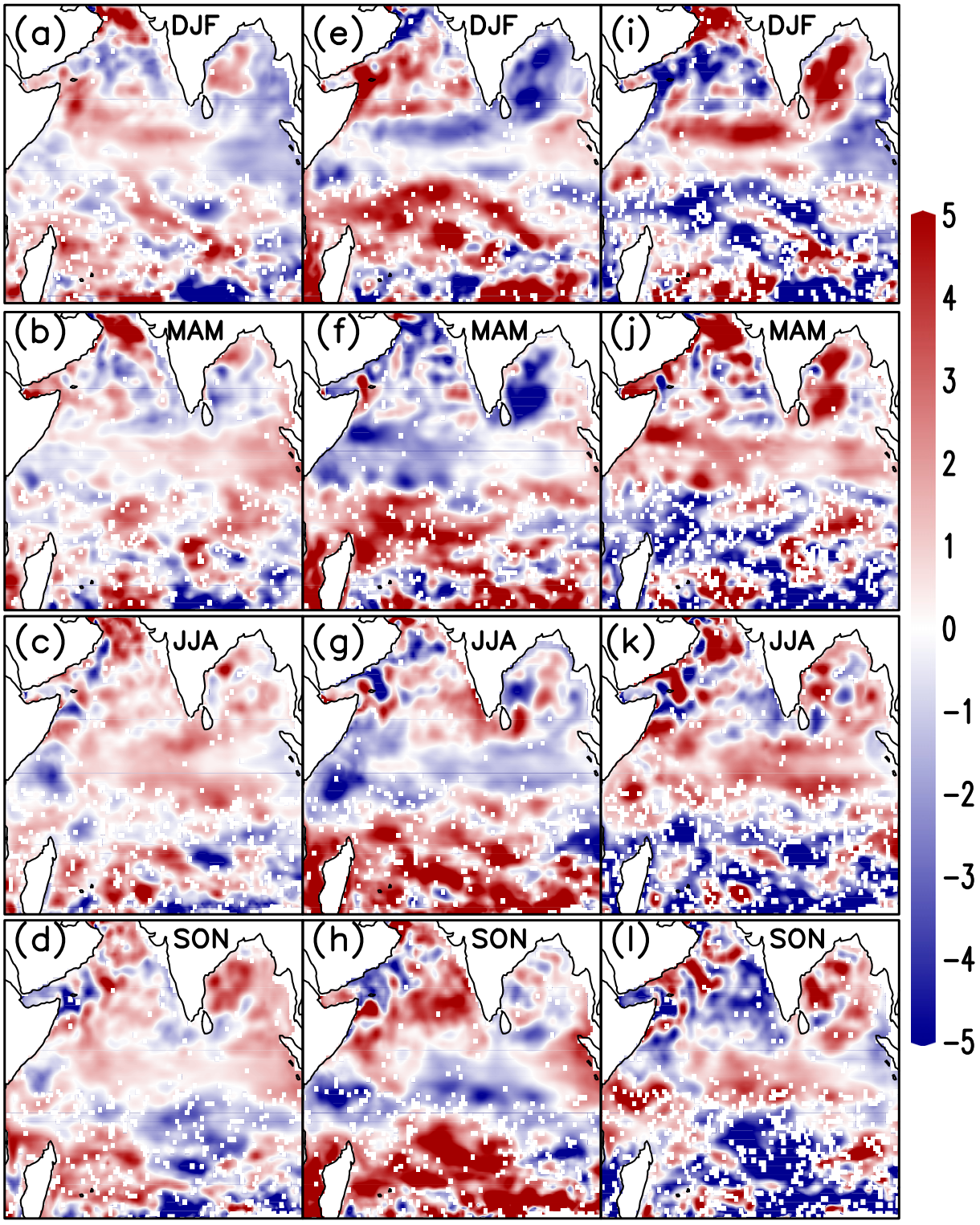

FIG. 8. The composite ocean heat content anomalies measured by the depth of 20°C (m) from SODA reanalysis for ISM seasons in the $Q1$ quadrant in Fig. 1 (canonical seasons) for (a) DJF, (b) preceding MAM, (c) contemporaneous JJA, and (d) following SON seasons. Similarly, ocean heat content anomalies from ISM seasons in $Q4$ quadrant in Fig. 1 (noncanonical seasons) for preceding (e) DJF and (f) MAM, (g) contemporaneous JJA, and (h) following SON seasons. (i)–(l) The corresponding composite difference in the ocean heat content anomalies between the $Q1$ and $Q4$ seasons. Only significant values at the 10% significance level are plotted.

fails to provide such information in the noncanonical seasons.

Our analysis reveals that a majority of the noncanonical ISM seasons are seasons with anomalously more seasonal rain but with comparatively shorter length than climatology. These ISM seasons usually occur in years when ENSO anomalies in the JJA season over the east Pacific are weak. But weak ENSO events are nondiscriminatory between canonical and noncanonical ISM seasons.

While the onsets of the noncanonical ISM seasons do seem to be weakly forced by the preceding winter ENSO forcing on the large-scale meridional temperature gradient, the comparatively stronger southwesterly flow than the comparable canonical seasons lead to a relative depletion of moist static energy over the season that leads to an early demise of the ISM season despite favorable ENSO forcing of large-scale temperature gradients for delayed demise. The stronger southwesterlies of the noncanonical seasons result in relatively more cooling of the northern Indian Ocean from more Ekman heat transport that ultimately reduces the moist static energy causing earlier demise than the canonical wet ISM seasons. Further sensitivity studies with numerical climate models may have to be pursued to understand the determinants of canonical and noncanonical ISM seasons under weak ENSO conditions. We conjecture that internal variability of the ISM could be dictating this behavior under weak external ENSO forcing.

Acknowledgments. We thank the three anonymous reviewers for their very useful review of the previous version of the manuscript. The authors gratefully acknowledge the financial support given by NOAA (NA12OAR4310078) and the Earth System Science Organization, Ministry of Earth Sciences, Government of India (Grant MM/SERP/FSU/2014/SSC-02/002), to conduct this research under Monsoon Mission. We also thank the Indian Meteorological Department for the availability of the daily rain analysis over India.

REFERENCES

Ananthakrishnan, R., and M. K. Soman, 1988: The onset of the southwest monsoon over Kerala: 1901–1980. *J. Climatol.*, **8**, 283–296, doi:10.1002/joc.3370080305.

Angell, J. K., 1981: Comparison of variations in atmospheric quantities with sea surface temperature variations in the equatorial eastern Pacific. *Mon. Wea. Rev.*, **109**, 230–243, doi:10.1175/1520-0493(1981)109<0230:COVIAQ>2.0.CO;2.

Carton, J. A., and B. S. Giese, 2008: A reanalysis of ocean climate using Simple Ocean Data Assimilation (SODA). *Mon. Wea. Rev.*, **136**, 2999–3017, doi:10.1175/2007MWR1978.1.

Chirokova, G., and P. J. Webster, 2006: Interannual variability of Indian Ocean heat transport. *J. Climate*, **19**, 1013–1031, doi:10.1175/JCLI3676.1.

Goswami, B. N., and P. K. Xavier, 2005: ENSO control on the South Asian monsoon through the length of the rainy season. *Geophys. Res. Lett.*, **32**, L18717, doi:10.1029/2005GL023216.

Kessler, W. S., 1990: Observations of long Rossby waves in the northern tropical Pacific. *J. Geophys. Res.*, **95**, 5183–5217, doi:10.1029/JC095iC04p05183.

Koteswaram, P., 1958: The easterly jet stream in the tropics. *Tellus*, **10A**, 43–57, doi:10.1111/j.2153-3490.1958.tb01984.x.

Krishnakumar, V., and K. M. Lau, 1998: Possible role of symmetric instability in the onset and abrupt transition of the Asian monsoon. *J. Meteor. Soc. Japan*, **76**, 363–383.

Krishnamurthy, V. K., and J. L. Kinter III, 2003: The Indian Monsoon and its relation to global climate variability. *Global Climate*, X. Rodo and F. A. Comin, Eds., Springer, 186–236.

Meinen, C. S., and M. J. McPhaden, 2000: Observations of warm water volume changes in the equatorial Pacific and their relationship to El Niño and La Niña. *J. Climate*, **13**, 3551–3559, doi:10.1175/1520-0442(2000)013<3551:OOWWVC>2.0.CO;2.

Misra, V., H. Li, and M. Kozar, 2014: The precursors in the Intra-Americas Seas to seasonal climate variations over North America. *J. Geophys. Res. Oceans*, **119**, 2938–2948, doi:10.1002/2014JC009911.

Mo, K. C., 2010: Interdecadal modulation of the impact of ENSO on precipitation and temperature over the United States. *J. Climate*, **23**, 3639–3656, doi:10.1175/2010JCLI3553.1.

Noska, R., and V. Misra, 2016: Characterizing the onset and demise of the Indian summer monsoon. *Geophys. Res. Lett.*, **43**, 4547–4554, doi:10.1002/2016GL068409.

Pai, D. S., L. Sridhar, M. Rajeevan, O. P. Sreejith, N. S. Satbhai, and B. Mukhopadhyay, 2014: Development of a new high spatial resolution (0.25° × 0.25°) long period (1901–2010) daily gridded rainfall data set over India and its comparison with existing data sets over the region. *Mausam*, **65**, 1–18.

——, ——, M. R. Badwaik, and M. Rajeevan, 2015: Analysis of the daily rainfall events over India using a new long period (1901–2010) high resolution (0.25° × 0.25°) gridded rainfall data set. *Climate Dyn.*, **45**, 755–776, doi:10.1007/s00382-014-2307-1.

Parker, D. J., P. Willets, C. Birch, A. G. Turner, J. H. Marsham, C. M. Taylor, S. Kolusu, and G. M. Martin, 2016: The interaction of moist convection and mid-level dry air in the advance of the onset of the Indian monsoon. *Quart. J. Roy. Meteor. Soc.*, **142**, 2256–2272, doi:10.1002/qj.2815.

Poli, P., and Coauthors, 2013: The data assimilation system and initial performance evaluation of the ECMWF pilot reanalysis of the 20th-century assimilating surface observations only (ERA-20C). ERA Rep. Series 14, 62 pp. [Available online at http://www.ecmwf.int/sites/default/files/elibrary/2013/11699-data-assimilation-system-and-initial-performance-evaluation-ecmwf-pilot-reanalysis-20th.pdf.]

Ramage, C., 1971: *Monsoon Meteorology*. International Geophysics Series, Vol. 15, Academic Press, 296 pp.

Shukla, J., and D. A. Paolino, 1983: The Southern Oscillation and long-range forecasting of the summer monsoon rainfall over India. *Mon. Wea. Rev.*, **111**, 1830–1837, doi:10.1175/1520-0493(1983)111<1830:TSOALR>2.0.CO;2.

Sikka, D. R., 1980: Some aspects of the large scale fluctuations of summer monsoon rainfall over India in relation to fluctuations in the planetary and regional scale circulation parameters. *Proc. Indian Acad. Sci., Earth Planet. Sci.*, **89**, 179–195, doi:10.1007/BF02913749.

Smith, T. M., R. W. Reynolds, T. C. Peterson, and J. Lawrimore, 2008: Improvements to NOAA's historical merged land–ocean surface temperature analysis (1880–2006). *J. Climate*, **21**, 2283–2296, doi:10.1175/2007JCLI2100.1.

Sperber, K. R., and H. Annamalai, 2014: The use of fractional accumulated precipitation for the evaluation of the annual cycle of monsoons. *Climate Dyn.*, **43**, 3219–3244, doi:10.1007/s00382-014-2099-3.

Tomas, R., and P. Webster, 1997: The role of inertial instability in determining the location and strength of near-equatorial convection. *Quart. J. Roy. Meteor. Soc.*, **123**, 1445–1482, doi:10.1002/qj.49712354202.

Webster, P. J., 2000: The coupled monsoon system. *The Asian Monsoon*, B. Wang, Ed., Springer, 3–66.

——, V. O. Magaña, T. N. Palmer, J. Shukla, R. A. Tomas, M. Yanai, and T. Yasunari, 1998: Monsoons: Processes, predictability, and the prospects for prediction. *J. Geophys. Res.*, **103**, 14 451–14 510, doi:10.1029/97JC02719.

Wilks, D. S., 2011: *Statistical Methods in the Atmospheric Sciences*. 3rd ed. International Geophysics Series, Vol. 100, Academic Press, 676 pp.

Xavier, P. K., C. Marzin, and B. N. Goswami, 2007: An objective definition of the Indian summer monsoon season and a new perspective on the ENSO–monsoon relationship. *Quart. J. Roy. Meteor. Soc.*, **133**, 749–764, doi:10.1002/qj.45.

Yadava, M. G., R. Ramesh, and G. B. Pant, 2004: Past monsoon rainfall variations in peninsular India recorded in a 331-year-old speleothem. *Holocene*, **14**, 517–524, doi:10.1191/0959683604hl728rp.

Yanai, M., C. Li, and Z. Song, 1992: Seasonal heating of the Tibetan Plateau and its effects on the evolution of the Asian summer monsoon. *J. Meteor. Soc. Japan*, **70**, 319–351.

Yuan, J., W. Li, and Y. Deng, 2015: Amplified subtropical stationary waves in boreal summer and their implications for regional water extremes. *Environ. Res. Lett.*, **10**, 104009, doi:10.1088/1748-9326/10/10/104009.